

Conduction-radiation interplay between two closely-separated solids

M. Reina, R. Messina, and P. Ben-Abdallah

*Laboratoire Charles Fabry, UMR 8501, Institut d'Optique, CNRS,
Université Paris-Saclay, 2 Avenue Augustin Fresnel, 91127 Palaiseau Cedex, France.*

(Dated: March 21, 2022)

In the theory of radiative heat exchanges between two closely-spaced bodies introduced by Polder and van Hove, no interplay between the heat carriers inside the materials and the photons crossing the separation gap is assumed. Here we release this constraint by developing a general theory to describe the conduction-radiation coupling between two solids of arbitrary size separated by a subwavelength separation gap. We show that, as a result of the temperature profile induced by the coupling with conduction, the radiative heat flux exchanged between two parallel slabs at nanometric distances can be several orders of magnitude smaller than the one predicted by the conventional theory. These results could have important implications in the fields of nanoscale thermal management, heat-assisted recording and nanoscale energy conversion.

PACS numbers: 44., 44.10.+i, 44.40.+a, 63.22.+m, 78.20.Nv

Understanding the radiative heat transfer between two bodies at different temperatures is a very old problem in physics. At long separation distance, where energy exchange results exclusively from propagative photons, this transfer is well described by the radiometry theory introduced by Schuster [1] and completed by the black-body theory of Planck [2] at the beginning of 20th century. On the other hand, at subwavelength distances (i.e. in the near-field regime) the situation radically changes. Indeed, at this scale evanescent photons become the main contributors to the heat transfer by tunneling effect through the separation gap [3]. The modeling of this transfer has found its completion in the '70s with the work of Polder and van Hove (PvH) [4], based on Rytov's theory of fluctuational electrodynamics [5]. In this semiclassical theory, the Poynting flux is calculated by summing up all the contributions generated by the random thermally-activated electric currents inside each body. This leads to the prediction of a dramatic amplification of radiative heat flux in the near field (with respect to the far field), which has been confirmed experimentally down to the nanometer range of distances considered in this work [6, 7].

In the PvH theory the net power exchanged between two solids held at uniform temperature is expressed in terms of the Fresnel coefficients of these bodies. In that sense this theory is a surface-exchange theory. Nevertheless, generally speaking thermal photons are transported throughout each body and they dissipate their energy unevenly through them. Consequently, the temperature field within each body is generally not uniform and its spatio-temporal variation is driven by the conduction-radiation coupling between the two bodies. A first attempt to describe this coupling has been proposed in 2016 [8]. However, this phenomenological approach was limited to bodies of characteristic length much larger than the mean free path of heat carriers, so that no ballistic or partially ballistic transport could be taken into

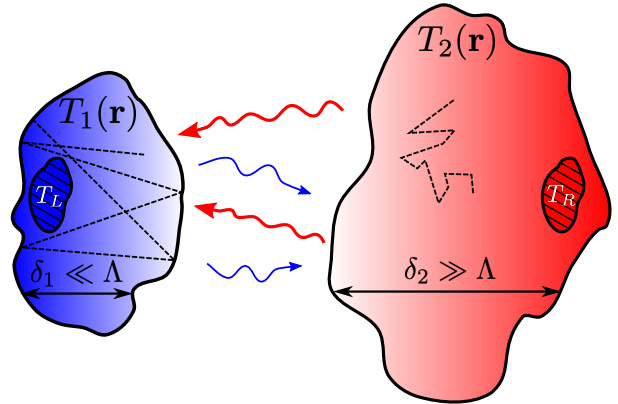


Figure 1: Sketch of two bodies of finite size at different temperatures, partially coupled to two thermostats (hatched areas) at temperature T_L and T_R , and exchanging heat radiatively through their separation gap. The black dashed lines show the heat-carrier (electron or phonon) trajectories between successive colliding events when the characteristic sizes δ_1 and δ_2 are respectively much smaller (i.e. ballistic regime) and much larger (i.e. diffusive regime) than the mean free path Λ . The temperature field $T_{1,2}(\mathbf{r})$ inside each body results from the local interplay between conduction and radiation.

account.

In this Letter we introduce a general theoretical framework to describe the heat transfer between two solids of arbitrary size by taking into account the interplay between conduction and radiation. The essence of this approach is based on the combination of Boltzmann's equation to deal with the transport of heat carriers inside the solids (valid for any heat-transport regime) and fluctuational electrodynamics to calculate the radiative power locally dissipated in each body.

To start, let us consider two bodies as sketched in Fig. 1, assumed to be in partial contact with two thermostats. The internal energy density u within these bod-

ies obeys the conservation equation

$$\frac{\partial u(\mathbf{r}, t)}{\partial t} = P_{\text{rad}}(\mathbf{r}, t) + P_{\text{cond}}(\mathbf{r}, t), \quad (1)$$

where P_{rad} denotes the radiative power locally dissipated per unit volume within a given body and coming from the other one, while P_{cond} is the conductive power per unit volume around the point \mathbf{r} , respectively. The latter can be calculated as the divergence of conductive flux

$$\varphi_{\text{cond}}(t, \mathbf{r}) = \sum_p \int_{4\pi} d\Omega \int d\omega \hbar\omega \mathbf{v}_{g,p}(\omega) f_p(t, \omega, \mathbf{r}, \Omega) \frac{D_p(\omega)}{4\pi}, \quad (2)$$

using the distribution function f associated to the heat carriers within the solid, the density of states $D_p(\omega)$, the group velocity $\mathbf{v}_{g,p}(\omega) = \nabla_{\mathbf{k}}\omega_p$ of carriers at the frequency ω and solid angle Ω . The distribution function f_p for each polarization state p can be calculated by solving Boltzmann's equation (for a given frequency ω , not shown for simplicity) under the relaxation time approximation

$$\frac{\partial f_p}{\partial t} + \mathbf{v}_{g,p} \cdot \nabla f_p = -\frac{f_p - f_0}{\tau_p(\omega, T(\mathbf{r}))}, \quad (3)$$

where f_0 is the equilibrium distribution (Fermi-Dirac for electrons and Bose-Einstein for phonons) and τ_p is the heat-carrier relaxation time.

Concerning the radiative power, we start by neglecting the energy exchanged between parts of the same slab, assuming that this contribution is negligible with respect to conduction. The power P_{rad}^L (resp. P_{rad}^R) dissipated in the left (resp. right) body and associated to the sources in the other body can be calculated from the net radiative flux φ_{rad}^R (resp. φ_{rad}^L) using the statistical average $\langle \mathbf{S}(\mathbf{r}, \omega) \rangle = 2 \text{Re} \langle \mathbf{E}(\mathbf{r}, \omega) \times \mathbf{H}^*(\mathbf{r}, \omega) \rangle$ of the Poynting vector spectrum at point \mathbf{r} as

$$P_{\text{rad}}^{L/R} = - \int d\omega \nabla \cdot \varphi_{\text{rad}}^{R/L}(\mathbf{r}, \omega). \quad (4)$$

According to the fluctuational-electrodynamics theory [5], the contribution to the Poynting vector coming from the sources located in the left or right body reads

$$\begin{aligned} \langle S_k^{R,L}(\mathbf{r}, \omega) \rangle &= i \frac{\omega^2}{c^2} \eta_{kjl} \int_{R,L} d\mathbf{r}' \epsilon''(\mathbf{r}', \omega) \Theta(T(\mathbf{r}'), \omega) \\ &\times [\mathbf{G}_{j,l}^{EE} \mathbf{G}_{k,l}^{EH*} - \mathbf{G}_{j,l}^{EH*} \mathbf{G}_{k,l}^{EE}], \end{aligned} \quad (5)$$

where $\Theta(T, \omega) = \hbar\omega / [e^{\frac{\hbar\omega}{k_B T}} - 1]$ is the mean energy of a Planck oscillator at temperature T , ϵ'' the imaginary part of the permittivity in the emitting body while $\mathbf{G}^{EE} = \mathbf{G}^{EE}(\mathbf{r}, \mathbf{r}')$ and $\mathbf{G}^{HE} = \mathbf{G}^{HE}(\mathbf{r}, \mathbf{r}')$ are the full electric-electric and electric-magnetic dyadic Green tensors at frequency ω , taking into account all scattering events within the system between the emitter and the point where energy is dissipated. When calculating the net radiative

power P_{rad} dissipated at position \mathbf{r} , we use Eq. (4) and finally replace $\Theta(T(\mathbf{r}'), \omega)$ by $\Theta(T(\mathbf{r}'), \omega) - \Theta(T(\mathbf{r}), \omega)$ in order to take into account the power emitted by the element located at \mathbf{r} and ensure vanishing energy exchange at thermal equilibrium.

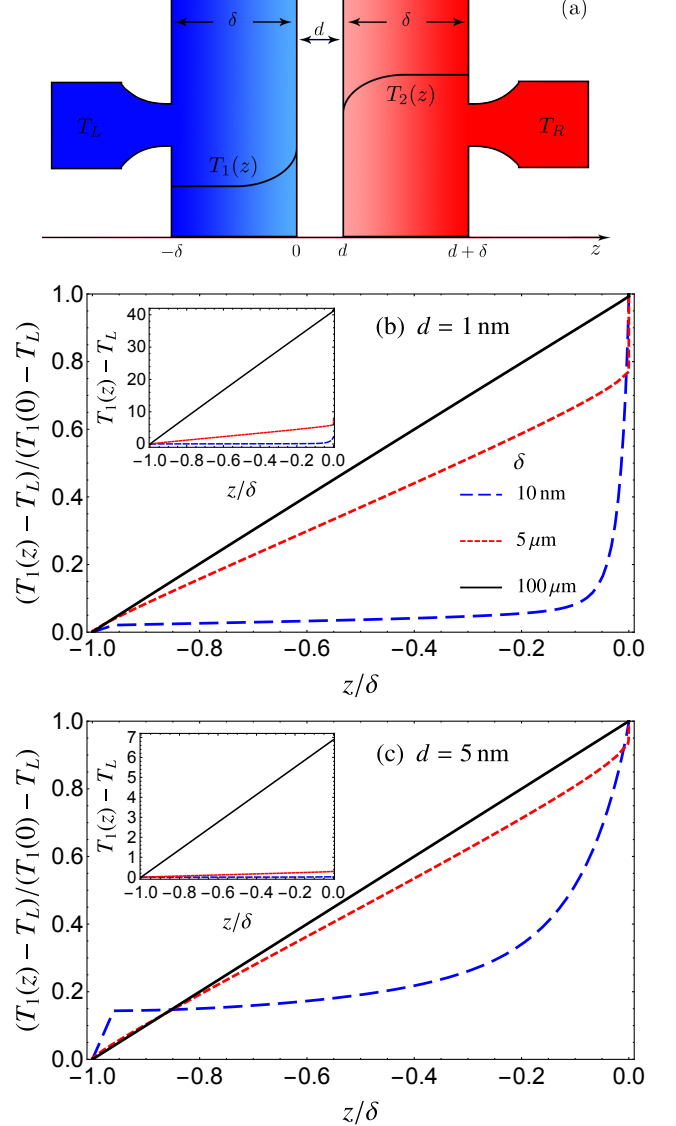


Figure 2: (a) Two parallel 3C-SiC slabs of thickness δ separated by a vacuum gap of thickness d and thermostated on their external sides at $T_L = 300$ K and $T_R = 400$ K. (b) Steady-state temperature (inset) and normalized temperature profile inside the left slab for different thicknesses and a separation distance $d = 1$ nm. (c) Same as (b) for $d = 5$ nm.

To illustrate the importance of coupling mechanism between conduction and radiation in a two-body system in near-field interaction, we focus on a simple configuration made of two identical slabs [Fig. 2(a)] of arbitrary thickness δ separated by a vacuum gap of thickness d , and in contact on their external sides with two thermostats at

temperature T_L and $T_R > T_L$. For the sake of clarity we consider slabs made of silicon carbide with a zincblende crystal structure (3C-SiC) and thicknesses larger than 10 nm, so that their dielectric permittivity can be assumed to be size-independent. Using the dispersion relation of acoustic modes (giving the leading contribution to heat conduction), making the common isotropic assumption for wave vectors and considering the [100] direction in the \mathbf{k} space, we calculate [9] the phonon relaxation time by taking into account the scattering by point impurities, the umklapp processes and the boundary scattering using Matthiessen's rule [10]

$$\tau^{-1}(\omega, T) = A\omega^4 + B\omega^2 T^3 + C, \quad (6)$$

where the coefficients $A = 2.1237 \times 10^{-45} \text{ s}^3$, $B = 4.397 \times$

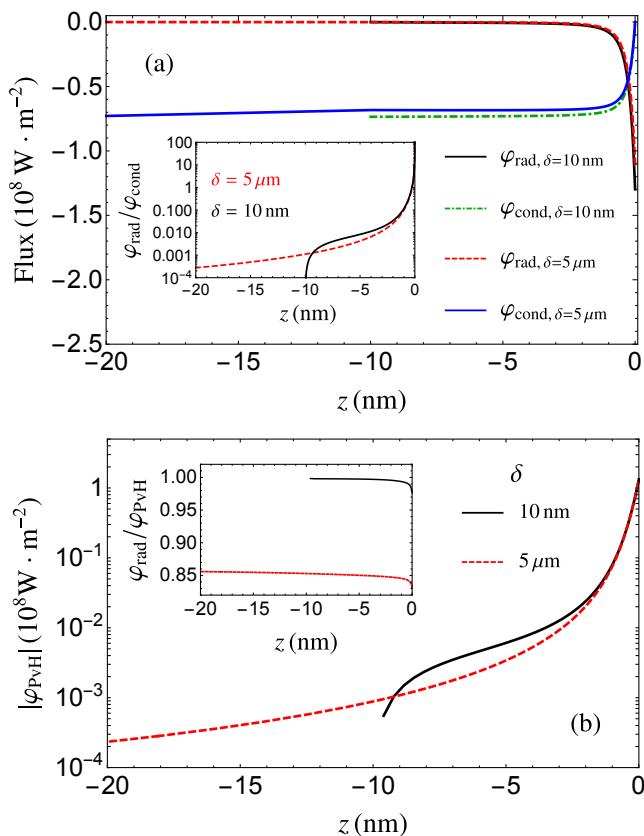


Figure 3: (a) Radiative flux φ_{rad} within the left slab in a system of two 3C-SiC slabs of thickness $\delta = 10 \text{ nm}$ and $\delta = 5 \mu\text{m}$ separated by a vacuum gap of thickness $d = 1 \text{ nm}$ and thermostated on their back sides at $T_L = 300 \text{ K}$ and $T_R = 400 \text{ K}$. Inset: ratio between φ_{rad} and the conductive flux φ_{cond} . (b) Absolute value of the PvH flux within the left slab for $\delta = 10 \text{ nm}$ and $\delta = 5 \mu\text{m}$ for a separation distance $d = 1 \text{ nm}$. Inset: ratio between the exact radiative flux φ_{rad} and the PvH prediction.

$10^{-25} \text{ s} \cdot \text{K}^{-3}$ and $C = 1.3949 \times 10^8 \text{ s}^{-1}$ have been obtained by fitting the simulated thermal conductivity [9] with the available experimental data [11] over the temperature

range $[T_L, T_R]$. Using this expression we can derive the power dissipated by conduction from Eq. (2). As for the radiative power, it can be calculated from Eq. (4) using the Green tensors in a multilayer geometry [12]. By neglecting the contribution of propagative photons we obtain [9]

$$P_{\text{rad}}(z) = \frac{2}{\pi^2} \sum_p \int_0^{+\infty} d\omega \int_{\frac{\omega}{c}}^{+\infty} dk k e^{-2\text{Im}(k_z)d} G(z, \omega) \times \int_0^\delta dz' \left(n[\omega, T(z' + d)] - n[\omega, T(-z)] \right) H(z', \omega), \quad (7)$$

where $n(\omega, T) = [e^{\frac{\hbar\omega}{k_B T}} - 1]^{-1}$ is the Bose-Einstein distribution function, while $G(z, \omega)$ and $H(z, \omega)$ are functions which depend on the optical properties of slabs [9].

The temperature profiles inside the slabs are obtained by solving through an iterative process Eq. (1) using the control angle discrete ordinates method [13] to solve Boltzmann's equation. For convenience, in the following we show temperature profiles in the left slabs, being the ones in the right slab qualitatively similar. The results in steady-state regime (i.e. for $\frac{\partial}{\partial t} \equiv 0$), are plotted in Fig. 2(b) for different slab thicknesses and a separation distance $d = 1 \text{ nm}$ (normalized in the main part to compare the different profile shapes, in real values in the inset). When the thickness is small ($\delta = 10 \text{ nm}$) compared to the mean free path of phonons [9] the regime of transport becomes ballistic. It follows that the temperature profile becomes almost constant and close to the reservoir temperature T_L (resp. T_R) in the left (resp. right) slab. Nevertheless, near the internal interfaces we note the presence of a sharp temperature variation. As shown in Fig. 3(a), this variation corresponds to the region where almost all the radiative energy carried by evanescent photons is deposited. This corresponds to the zone where the radiation-conduction coupling effectively takes place. As shown in the inset of Fig. 3(a) we see that for such thicknesses the radiative flux surpasses the conductive flux by two orders of magnitude close to the interface. Therefore, the phonons cannot cool down this region through their coupling with the external reservoir. As a result, the slab is significantly heated up locally (within some nm) close to the interface. On the other hand, beyond this region the conductive flux dominates the rapidly decaying radiative flux, so that the atomic lattice is thermalized at the reservoir temperature thanks to the ballistic phonons. For thicker slabs ($\delta > 5 \mu\text{m}$), we see in the inset of Fig. 3(a) that the radiative flux still dominates over the conductive one within a few nm from the vacuum interface. However, in this case the regime of conduction tends to be diffusive and the atomic lattice does not thermalize anymore at the reservoir temperature. The temperature profile decays gradually (linearly for a purely diffusive regime) to the reservoir temperature

thanks to the local colliding events of phonons. Figure 2(c) shows the results for a larger separation distance ($d = 5$ nm). While the overall qualitative behavior remains the same, the temperature drop is much smaller, due to the $1/d^2$ decay of the radiative flux. Also we note that the local radiative heating takes place at greater depth within the slab, the wave vectors of smaller value being preponderant for this separation distance.

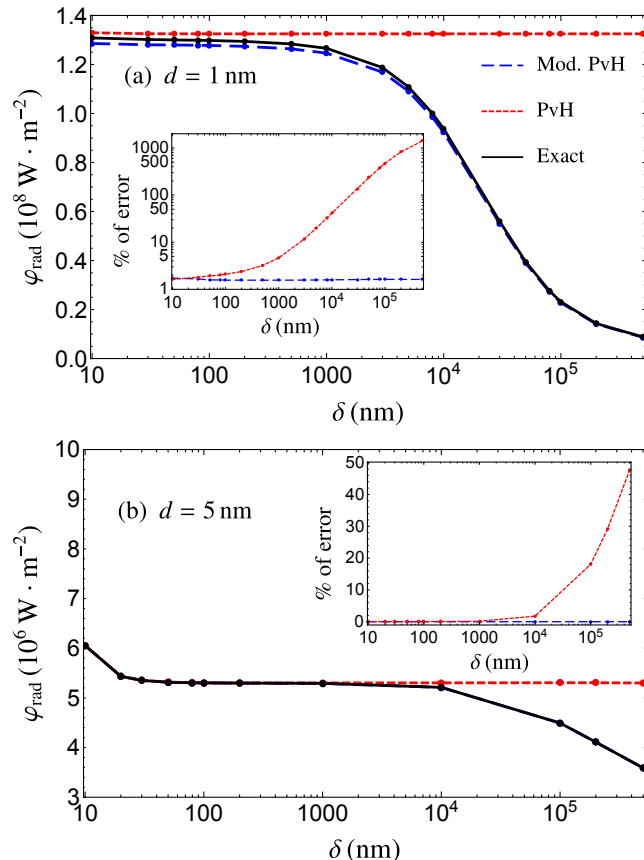


Figure 4: Radiative heat flux exchanged between two 3C-SiC slabs with respect to their thickness for a separation distance of (a) $d = 1$ nm and (b) $d = 5$ nm. We show the exact result (black line), the PvH one (red dashed line, uniform temperatures $T_L = 300$ K and $T_R = 400$ K) and the modified PvH flux (blue long-dashed line, uniform temperatures equal to the temperatures at the boundaries with the vacuum gap in the steady states resulting from the coupling with conduction). Insets: absolute value of the error with respect to the PvH and modified PvH approaches.

We now want to address the impact of conduction/radiation coupling on the value of radiative flux. We first focus on the spatial distribution of radiative flux φ_{rad} within the left slab. The results predicted by the PvH theory for two slabs set at uniform temperatures $T_L = 300$ K and $T_R = 400$ K are shown in Fig. 3(b) inside the first 20 nm from the vacuum gap. For the three considered thicknesses the flux is rapidly decaying and its value is almost the same over the first 2 nm. The inset

shows the ratio between the exact value of the flux (taking into account the radiation/conduction coupling mechanism) and the PvH predictions. While for $\delta = 10$ nm the PvH description is reliable, for higher thicknesses it largely overestimates the exact flux, as a result of the conduction-induced temperature profile.

We finally focus on the net radiative flux exchanged between the two slabs and compare it to the flux predicted by the PvH theory when the two bodies are held at uniform temperature. More specifically, we compare the exact flux to the PvH one with $T_L = 300$ K and $T_R = 400$ K, and to the PvH result using as slab temperatures the values of the temperatures at the boundaries with the vacuum gap in the steady states derived from our approach. The latter is referred as *modified PvH*. At 1 nm separation distance [Fig.4(a)], we see that for slab thicknesses larger than about $1 \mu\text{m}$ the discrepancy between the PvH prediction and our theory increases dramatically. The relative error is close to 5% when $\delta = 1 \mu\text{m}$ and scales as δ^2 beyond this thickness. In slabs of such thicknesses the regime of heat transport becomes almost diffusive (see the phonon mean free path in [9]) and the difference with the PvH theory comes from the linear variation of temperature profile which significantly reduces the temperature difference between the slabs. With thinner slabs the difference between the exact and the PvH theory becomes less pronounced, despite the temperature drop close to the internal interfaces highlighted previously. Nevertheless in these cases a relative error of about 2% persists. Focusing on the modified PvH result, we note that it pretty well reproduces the exact results for any slab thickness. This demonstrates that the heat transfer between two solids in the extreme near field is mainly a surface-interaction mechanism. When the separation distance is increased to $\delta = 5$ nm we see [Fig. 4(b)] that for thin slabs (i.e. ballistic regime) the predictions of the PvH theory match perfectly well the exact calculation. In this case the radiative coupling between the two slabs is significantly smaller than at $d = 1$ nm, so that the induced temperature gradient is much smaller [see Fig. 2(b)]. In this scenario, we only see a discrepancy with respect to the PvH results for large thicknesses, whereas the agreement with the modified PvH results is almost perfect.

In conclusion, we have introduced a general theory to describe heat exchanges between two closely-spaced solids of arbitrary size. Our theory takes into account the conduction-radiation coupling between the two bodies, not included in PvH theory. By applying our formalism to parallel planar slabs, we have shown that this coupling produces a temperature profile within each body, resulting in a radiative flux which can differ significantly from the one predicted by the PvH theory. This theory can be relevant in the modelling of experiments exploring heat transfer in the extreme near-field regime. It allows for a better temperature and heat-flux control at nanoscale and could find applications in the fields of nanoscale

thermal management, heat-assisted data recording and nanoscale energy conversion.

-
- [1] A. Schuster, *Radiation through a foggy atmosphere*, *Astrophys. J.* **21**, 1 (1905).
- [2] M. Planck, *The Theory of Heat Radiation* (Dover, New York, 1991).
- [3] K. Joulain, J.-P. Mulet, F. Marquier, R. Carminati, and J.-J. Greffet, *Surface electromagnetic waves thermally excited: Radiative heat transfer, coherence properties and Casimir forces revisited in the near field*, *Surf. Sci. Rep.* **57**, 59 (2005)
- [4] D. Polder and M. van Hove, *Theory of Radiative Heat Transfer between Closely Spaced Bodies*, *Phys. Rev. B* **4**, 3303 (1971).
- [5] S. M. Rytov, Y. A. Kravtsov, and V. I. Tatarskii, *Principles of Statistical Radiophysics*, Vol. 3 (Springer, New York, 1989).
- [6] K. Kloppstech, N. Köhne, S.-A. Biehs, A. W. Rodriguez, L. Worbes, D. Hellmann, and A. Kittel, *Giant heat transfer in the crossover regime between conduction and radiation*, *Nat. Commun.* **8**, 14475 (2017).
- [7] L. Cui, W. Jeong, V. Fernandez-Hurtado, J. Feist, F. J. Garcia-Vidal, J. C. Cuevas, E. Meyhofer, and P. Reddy, *Study of radiative heat transfer in Ångström- and nanometre-sized gaps*, *Nat. Commun.* **8**, 14479 (2017).
- [8] R. Messina, W. Jin, and A. W. Rodriguez, *Strongly coupled near-field radiative and conductive heat transfer between planar bodies*, *Phys. Rev. B* **94**, 121410(R) (2016).
- [9] See Supplemental Material at [URL will be inserted by publisher] for the description of basic properties of phonons in silicon carbide and of radiative heat transfer between planar media with a temperature profile.
- [10] Y.-J. Han and P. G. Klemens, *Anharmonic thermal resistivity of dielectric crystals at low temperatures*, *Phys. Rev. B* **48**, 6033 (1993).
- [11] D. Morelli, J. Heremans, C. Beetz, W. S. Woo, G. Harris, and C. Taylor, *Carrier concentration dependence of the thermal conductivity of silicon carbide*, *Institute of Physics Conference Series* **137**, 313 (1994).
- [12] M. S. Tomáš, *Green function for multilayers: Light scattering in planar cavities*, *Phys. Rev. A* **51** 2545 (1995).
- [13] S. A. Ali and S. Mazumder, *Phonon Heat Conduction in Multidimensional Heterostructures: Predictions Using the Boltzmann Transport Equation*, *J. Heat Transfer* **137**, 102401 (2015).